

Control of Structures and Sorption Properties of Ionic Crystals of  $A_2[Cr_3O(OOCC_2H_5)_6(H_2O)_3]_2[\alpha-SiW_{12}O_{40}]$  ( $A = Na, K, Rb, NH_4, Cs, TMA$ )

Aldes Lesbani, Ryosuke Kawamoto, Sayaka Uchida, and Noritaka Mizuno\*

Department of Applied Chemistry, School of Engineering, The University of Tokyo, 7-3-1 Hongo, Bunkyo-ku, Tokyo 113-8656, Japan

Received November 28, 2007

The complexation of Keggin-type polyoxometalate  $[\alpha-SiW_{12}O_{40}]^{4-}$ , macrocation  $[Cr_3O(OOCC_2H_5)_6(H_2O)_3]^+$ , and monovalent cation  $A^+$  forms ionic crystals of  $A_2[Cr_3O(OOCC_2H_5)_6(H_2O)_3]_2[\alpha-SiW_{12}O_{40}] \cdot nH_2O$  ( $A = Na$  (**1a**),  $K$  (**2a**),  $Rb$  (**3a**),  $NH_4$  (**4a**),  $Cs$  (**5a**), and tetramethylammonium (TMA) (**6a**)). Single crystal (**1a–4a** and **6a**) and powder (**5a**) X-ray analyses have shown that the ionic crystals possess 2D layers of polyoxometalates and macrocations. Compounds **2a–5a** had almost the same structure, while the layers in **1a** and **6a** stack in different ways. The structures and sorption properties of **2b–5b** are investigated in more detail. The interlayer distances of guest free phases **2b–5b** increase with the increase in the ionic radii of the monovalent cations, which reside between the layers. Compounds **2b–5b** possess hydrophobic and hydrophilic channels, which exist between the layers and through the layers, respectively. The volumes of the hydrophobic channels increase in the order of  $2b < 3b \approx 4b < 5b$ , and those of the hydrophilic channels increase in the order of  $2b \leq 3b \leq 4b < 5b$ . Single-crystal X-ray structure analyses of **2a–4a** have shown that the water of crystallization resides in the hydrophilic channel. It is probable that the water of crystallization in **5a** resides in the hydrophilic channel in the same manner as those in **2a–4a** since **2a–5a** have almost the same structure. The water vapor sorption profiles of **2b–5b** are approximately reproduced by a linear driving force model. Therefore, water molecules sorbed in **2b–5b** probably reside in the hydrophilic channel. The *n*-propanol sorption profiles are reproduced by the summation of the linear driving force model, showing that two independent barriers exist in the *n*-propanol sorption. The in situ IR spectra of *n*-propanol sorbed showed the presence of two *n*-propanol species. These data show that *n*-propanol is sorbed into both hydrophilic and hydrophobic channels. Compound **5b** sorbs halocarbons in the hydrophobic channel, while **2b–4b** exclude them.

## Introduction

Remarkable progress has recently been made in the construction of crystalline solids, which are applicable to selective sorption, separation, and heterogeneous catalysis.<sup>1</sup> The control of porosity (pore size, dimension, surface, etc.) of the crystalline solids is essential to develop novel sorption properties.<sup>1</sup> Microporous zeolites possess anionic frame-

works, and the pore sizes can be controlled by those of the counter cations in the pore.<sup>2</sup> For example, the pore sizes of K-A and Na-A zeolites are 3 and 4 Å, respectively.<sup>2a</sup> The pore sizes and surface properties of metal-organic frameworks can be controlled by the lengths and kinds of the functional groups of the organic ligands.<sup>1</sup> For example, the pore sizes of isostructural zinc–benzenedicarboxylate<sup>3</sup> and zinc–triphenyldicarboxylate<sup>4</sup> are 1.3 and 2.9 nm, respec-

\* To whom correspondence should be addressed. E-mail: tmizuno@mail.ecc.u-tokyo.ac.jp. Fax: +81-3-5841-7220. Phone: +81-3-5841-7272.

(1) (a) Barton, T. J.; Bull, L. M.; Klemperer, W. G.; Loy, P. A.; McEnaney, B.; Misono, M.; Monson, P. A.; Pez, G.; Scherer, G. W.; Vartuli, J. C.; Yaghi, O. M. *Chem. Mater.* **1999**, *11*, 2633. (b) Yaghi, O. M.; O’Keeffe, M.; Ockwig, N. W.; Chae, H. K.; Eddaoudi, M.; Kim, J. *Nature* **2003**, *423*, 705. (c) Kitagawa, S.; Kitaura, R.; Noro, S. *Angew. Chem., Int. Ed.* **2004**, *43*, 2334. (d) Fletcher, A. J.; Thomas, K. M.; Rosseinsky, M. J. *J. Solid State Chem.* **2007**, *178*, 2491. (e) Serre, C.; Mellot-Drazniewski, C.; Surlé, S.; Audebrand, N.; Filinchuk, Y.; Férey, G. *Science* **2007**, *315*, 1828.

(2) (a) Breck, D. W.; Eversole, W. G.; Milton, R. M.; Reed, T. B.; Thomas, T. L. *J. Am. Chem. Soc.* **1956**, *78*, 5963. (b) Kuznicki, S. M.; Bell, V. A.; Nair, S.; Hillhouse, H. W.; Jacobinas, R. M.; Braunbarth, C. M.; Toby, B. H.; Tsapatsis, M. *Nature* **2001**, *412*, 720. (c) Davis, M. E. *Nature* **2002**, *417*, 813. (d) Corma, A.; Díaz-Cabañas, M. J.; Jordá, J. L.; Martínez, C.; Moliner, M. *Nature* **2006**, *443*, 842.

(3) Rosi, N. L.; Eckert, J.; Eddaoudi, M.; Vodak, D. T.; Kim, J.; O’Keeffe, M.; Yaghi, O. M. *Science* **2003**, *300*, 1127.

(4) Chae, H. K.; Siberio-Pérez, D. Y.; Kim, J.; Go, Y.; Eddaoudi, M.; Matzger, A. J.; O’Keeffe, M.; Yaghi, O. M. *Nature* **2004**, *427*, 523.

tively. The incorporation of free hydroxyl groups in the organic ligands of metal-organic frameworks increases the hydrophilicity.<sup>5</sup> As for clays, interlayer cations play an important role in the sorption, and IR studies show that the magnitude of host-guest interaction increases with the increase in the electron density of the interlayer cations.<sup>6</sup>

Polyoxometalates are nanosized metal-oxygen macroanions and suitable building blocks of nanostructured ionic crystals in combination with appropriate macrocations.<sup>7,8</sup> We have recently reported the structures and sorption properties of  $A_2[Cr_3O(OOCC_2H_5)_6(H_2O)_3]_2[\alpha-SiW_{12}O_{40}]$  ( $A = K, Cs$ ).<sup>9,10</sup> These ionic crystals are composed of 2D layers of polyoxometalates and macrocations, and monovalent cations reside between the adjacent layers. The interlayer distance increases from  $A = K$  to larger  $Cs$ . In this work, we have attempted to incorporate various monovalent cations,  $Na^+$  (radius, 1.16 Å),  $K^+$  (1.52 Å),  $Rb^+$  (1.66 Å),  $NH_4^+$  (1.66 Å),  $Cs^+$  (1.81 Å), and  $TMA^+$  (2.15 Å), and investigated the effects of the monovalent cations on the structures and sorption properties.

## Experimental Section

**Syntheses of Ionic Crystals 1a–6a.**  $Na_2[Cr_3O(OOCC_2H_5)_6(H_2O)_3]_2[\alpha-SiW_{12}O_{40}] \cdot 6H_2O$  (**1a**) was synthesized as follows:  $H_4[\alpha-SiW_{12}O_{40}] \cdot nH_2O^{11}$  (1.0 g, 0.35 mmol) was dissolved into 10 mL of water, and  $[Cr_3O(OOCC_2H_5)_6(H_2O)_3](NO_3) \cdot nH_2O^{12}$  (0.10 g, 0.14 mmol) was added with stirring, followed by the addition of  $NaCl$  (1.0 g, 17 mmol). The solution was kept at room temperature for 1 day. Green crystals of **1a** were isolated in 30% yield (based on macrocation). FT-IR spectrum (KBr): 1602, 1534, 1469, 1442,

1378( $\nu_{sym}(OCO)$ ), 1307, 1092, 1016, 972( $\nu_{asym}(W=O)$ ), 921( $\nu_{asym}(Si-O)$ ), 886( $\nu_{asym}(W-Oc-W)$ ), 803( $\nu_{asym}(W-Oe-W)$ ), 652( $\nu_{asym}(Cr-O)$ )  $cm^{-1}$ . Elemental analysis calcd for **1a**: C, 9.92; H, 1.94; Na, 1.06; Si, 0.65; Cr, 7.16; W, 50.63. Found: C, 10.63; H, 2.24; Na, 1.15; Si, 0.65; Cr, 7.33; W, 50.71.

The ionic crystal of  $K_2[Cr_3O(OOCC_2H_5)_6(H_2O)_3]_2[\alpha-SiW_{12}O_{40}] \cdot 4H_2O$  (**2a**) was synthesized according to ref 9.

$Rb_2[Cr_3O(OOCC_2H_5)_6(H_2O)_3]_2[\alpha-SiW_{12}O_{40}] \cdot 4H_2O$  (**3a**) was synthesized as follows:  $H_4[\alpha-SiW_{12}O_{40}] \cdot nH_2O^{11}$  (0.30 g, 0.10 mmol) was dissolved into 9 mL of water, and  $[Cr_3O(OOCC_2H_5)_6(H_2O)_3](NO_3) \cdot nH_2O^{12}$  (0.30 g, 0.41 mmol) was added with stirring, followed by the addition of  $RbCl$  (0.03 g (0.25 mmol) in 2 mL of water). The solution was kept at room temperature for 1 day. Green crystals of **3a** were isolated in 64% yield (based on polyoxometalate). FT-IR spectrum (KBr): 1600, 1534, 1468, 1442, 1378 ( $\nu_{sym}(OCO)$ ), 1307, 1091, 1016, 971( $\nu_{asym}(W=O)$ ), 921( $\nu_{asym}(Si-O)$ ), 886( $\nu_{asym}(W-Oc-W)$ ), 802( $\nu_{asym}(W-Oe-W)$ ), 651( $\nu_{asym}(Cr-O)$ ). Elemental analysis calcd for **3a**: C, 9.89; H, 1.66; Rb, 3.91; Si, 0.64; Cr, 7.13; W, 50.44. Found: C, 9.77; H, 1.82; Rb, 3.80; Si, 0.59; Cr, 7.04; W, 49.90.

$(NH_4)_2[Cr_3O(OOCC_2H_5)_6(H_2O)_3]_2[\alpha-SiW_{12}O_{40}] \cdot 4H_2O$  (**4a**) was synthesized as follows:  $H_4[\alpha-SiW_{12}O_{40}] \cdot nH_2O^{11}$  (0.50 g, 0.17 mmol) was dissolved into 10 mL of water, and  $[Cr_3O(OOCC_2H_5)_6(H_2O)_3](NO_3) \cdot nH_2O^{12}$  (0.30 g, 0.41 mmol) was added, followed by the addition of  $NH_4Cl$  (0.10 g (1.9 mmol) in 2 mL of water). The solution was kept at room temperature for 6 h. Green crystals of **4a** were isolated in 33% yield (based on polyoxometalate). FT-IR spectrum (KBr): 1601, 1535, 1469, 1442, 1378 ( $\nu_{sym}(OCO)$ ), 1307, 1244, 1092, 1015, 968( $\nu_{asym}(W=O)$ ), 920( $\nu_{asym}(Si-O)$ ), 886( $\nu_{asym}(W-Oc-W)$ ), 803( $\nu_{asym}(W-Oe-W)$ ), 650( $\nu_{asym}(Cr-O)$ )  $cm^{-1}$ . Elemental analysis calcd for **4a**: C, 10.20; H, 1.90; N, 0.66; Si, 0.66; Cr, 7.36; W, 52.04. Found: C, 9.96; H, 2.20; N, 0.57; Si, 0.68; Cr, 7.42; W, 52.36.

$Cs_2[Cr_3O(OOCC_2H_5)_6(H_2O)_3]_2[\alpha-SiW_{12}O_{40}] \cdot 4H_2O$  (**5a**) was synthesized as follows:  $H_4SiW_{12}O_{40} \cdot nH_2O^{11}$  (0.18 g, 0.06 mmol) and  $LiOH$  (0.01 g, 0.24 mmol) were dissolved in 5 mL of water (solution A).  $[Cr_3O(OOCC_2H_5)_6(H_2O)_3](NO_3) \cdot nH_2O^{12}$  (0.75 g, 1.00 mmol) and  $CsCl$  (0.1 g, 0.06 mmol) were dissolved in 5 mL of water (solution B). Solution A was heated (368 K), and solution B was added with stirring followed by the formation of **5a** within 1 min in 85% yield (based on cesium ion). FT-IR spectrum (KBr): 1603, 1534, 1469, 1442, 1378( $\nu_{sym}(OCO)$ ), 1306, 1090, 1015, 970( $\nu_{asym}(W=O)$ ), 921( $\nu_{asym}(Si-O)$ ), 886( $\nu_{asym}(W-Oc-W)$ ), 803( $\nu_{asym}(W-Oe-W)$ ), 652( $\nu_{asym}(Cr-O)$ )  $cm^{-1}$ . Elemental analysis calcd for **5a**: C, 9.56; H, 1.74; Cr, 6.90; Cs, 5.88; Si, 0.62; W, 48.78. Found: C, 10.02; H, 1.90; Cr, 6.83; Cs, 5.85; Si, 0.61; W, 49.37.

$TMA_2[Cr_3O(OOCC_2H_5)_6(H_2O)_3]_2[\alpha-SiW_{12}O_{40}] \cdot 8H_2O$  (**6a**) was synthesized as follows:  $H_4[\alpha-SiW_{12}O_{40}] \cdot nH_2O^{11}$  (0.50 g, 0.17 mmol) was dissolved into 10 mL of water, and  $[Cr_3O(OOCC_2H_5)_6(H_2O)_3](NO_3) \cdot nH_2O^{12}$  (0.45 g, 0.62 mmol) was added with stirring, followed by the addition of  $TMAcI$  (0.03 g, 0.27 mmol). The solution was kept at room temperature for 6 h. Green crystals of **6a** were isolated in 69% yield (based on polyoxometalate). FT-IR spectrum (KBr): 1608, 1533, 1469, 1443, 1383( $\nu_{sym}(OCO)$ ), 1307, 1091, 1014, 971( $\nu_{asym}(W=O)$ ), 923( $\nu_{asym}(Si-O)$ ), 885( $\nu_{asym}(W-Oc-W)$ ), 802( $\nu_{asym}(W-Oe-W)$ ), 653( $\nu_{asym}(Cr-O)$ )  $cm^{-1}$ . The characteristic IR bands of  $TMA^+$  overlapped with the strong bands of the propionate ligand of the macrocation and polyoxometalate. Elemental analysis calcd for **6a**: C, 11.76; H, 2.51; N, 0.62; Si, 0.62; Cr, 6.94; W, 49.07. Found: C, 11.97; H, 2.43; N, 0.60; Si, 0.62; Cr, 7.08; W, 47.44.

- (5) Kitaura, R.; Fujimoto, K.; Noro, S.; Kondo, M.; Kitagawa, S. *Angew. Chem., Int. Ed.* **2002**, *41*, 133.
- (6) Yamanaka, S.; Kanamaru, F.; Koizumi, M. *J. Phys. Chem.* **1974**, *78*, 42.
- (7) Reviews on polyoxometalates: (a) Pope, M. T.; Müller, A. *Angew. Chem., Int. Ed. Engl.* **1991**, *30*, 34. (b) Hill, C. L.; Prosser-McCarthy, C. M. *Coord. Chem. Rev.* **1995**, *143*, 407. (c) Okuhara, T.; Mizuno, N.; Misono, M. *Adv. Catal.* **1996**, *41*, 113. (d) Hill, C. L. *Chem. Rev.* **1998**, *98*, 1. (e) Yamase, T.; Pope, M. T., Eds. *Polyoxometalate Chemistry for Nano-Composite Design*; Kluwer: Dordrecht, The Netherlands, 2002. (f) Kozhevnikov, I. V. *Catalysis by Polyoxometalates*; Wiley: Chichester, UK, 2002. (g) Hill, C. L. In *Comprehensive Coordination Chemistry II*; McClerverty, J. A., Meyer, T. J., Eds.; Elsevier: Amsterdam, 2003; p 679. (h) Neumann, R. In *Modern Oxidation Methods*; Bäckvall, J. E., Ed.; Wiley-VCH: Weinheim, Germany, 2004; p 223. (i) Mizuno, N.; Kamata, K.; Yamaguchi, K. *Surface and Nanomolecular Catalysis*; Taylor and Francis Group, LLC: New York, 2006; p 463.
- (8) Recent reports on nanostructured polyoxometalate compounds: (a) Hayashi, Y.; Müller, F.; Lin, Y.; Miller, S. M.; Anderson, O. P.; Finke, R. G. *J. Am. Chem. Soc.* **1997**, *119*, 11401. (b) Khan, M. I.; Yohannes, E.; Powell, D. *Inorg. Chem.* **1999**, *38*, 212. (c) Hagrman, D.; Hagrman, P. J.; Zubieta, J. *Angew. Chem., Int. Ed.* **1999**, *38*, 3165. (d) Son, J. H.; Choi, H.; Kwon, Y. U. *J. Am. Chem. Soc.* **2000**, *122*, 7432. (e) Schmitt, W.; Baissa, E.; Mandel, A.; Anson, C. E.; Powell, A. K. *Angew. Chem., Int. Ed.* **2001**, *40*, 3577. (f) Ishii, Y.; Takenaka, Y.; Konishi, K. *Angew. Chem., Int. Ed.* **2004**, *43*, 2702. (g) Vasylyev, M. V.; Neumann, R. *J. Am. Chem. Soc.* **2004**, *126*, 884. (h) Mal, S. S.; Kortz, U. *Angew. Chem., Int. Ed.* **2005**, *44*, 3777. (i) Streb, C.; Long, D. L.; Cronin, L. *Chem. Commun.* **2007**, 471. (j) Tan, H.; Li, Y.; Zhang, Z.; Qin, C.; Wang, X.; Wang, E. *J. Am. Chem. Soc.* **2007**, *129*, 10066.
- (9) Kawamoto, R.; Uchida, S.; Mizuno, N. *J. Am. Chem. Soc.* **2005**, *127*, 10560.
- (10) Jiang, C.; Lesbani, A.; Kawamoto, R.; Uchida, S.; Mizuno, N. *J. Am. Chem. Soc.* **2006**, *128*, 14240.
- (11) Téze, A.; Hervé, G. *Inorg. Synth.* **1990**, *27*, 93.
- (12) Fujihara, T.; Aonohata, J.; Kumakura, S.; Nagasawa, A.; Murakami, K.; Ito, T. *Inorg. Chem.* **1998**, *37*, 3779.

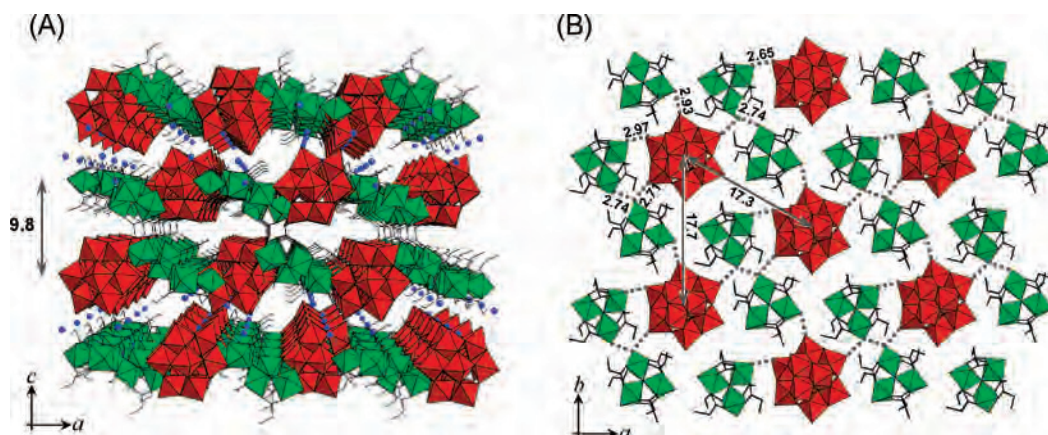


**Figure 1.** Crystal structure of  $Na_2[Cr_3O(OOCC_2H_5)_6(H_2O)_3]_2[\alpha-SiW_{12}O_{40}] \cdot 6H_2O$  [**1a**]. Perspective view (A) and arrangements of the constituent ions in the layer (B). Red, green, and orange polyhedra show the  $[WO_6]$ ,  $[CrO_6]$ , and  $[SiO_4]$ , respectively. Blue spheres show the sodium ions. Black sticks show the carbon chains. The water of crystallization was omitted for the clarity. Dotted lines in panel B show the hydrogen bonds in the layer.

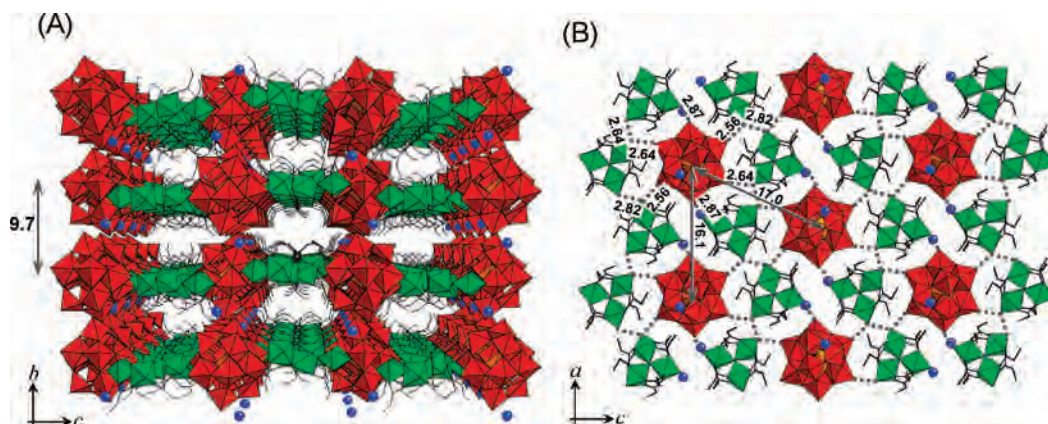


**Figure 2.** Crystal structure of  $Rb_2[Cr_3O(OOCC_2H_5)_6(H_2O)_3]_2[\alpha-SiW_{12}O_{40}] \cdot 4H_2O$  [**3a**]. Perspective view (A) and arrangements of the constituent ions in the layer (B). Red, green, and orange polyhedra show the  $[WO_6]$ ,  $[CrO_6]$ , and  $[SiO_4]$ , respectively. Blue spheres show the rubidium ions. Black sticks show the carbon chains. The water of crystallization was omitted for the clarity. Dotted lines in panel B show the hydrogen bonds in the layer.

**Preparation of Guest-Free Phases 2b–5b.** The water of crystallization in **2a–5a** was desorbed by the evacuation or treatment in a dry  $N_2$  flow at 303 K to form the corresponding guest-free phases **2b–5b**. It was confirmed by the TG-MS measurements that only water molecules were desorbed by the treatments. The weight losses of **2a–5a** by the evacuation or treatment in a dry  $N_2$  flow fairly agreed with the amounts of the water of crystallization in **2a–5a**. The IR spectrum of **2b–5b** showed the bands characteristic of the macrocation and polyoxometalate, showing that the molecular structures of the constituent ions are retained upon the desorption of the water of crystallization.

**Single-Crystal X-ray Analyses.** Single-crystal X-ray diffraction measurements were performed on a Rigaku Saturn diffractometer with graphite monochromated  $Mo\ K\alpha$  radiation ( $\lambda = 0.71070\ \text{\AA}$ ) and a CCD 2-D detector at 153 K (**1a–4a** and **6a**) or 303 K (**2b** and **3b**). The unit cell was determined from the reflections collected on the setting angles of seven frames by changing  $0.5^\circ$  for each frame. Two different settings were used, and the angles were changed by  $0.5^\circ$  per frame. Intensity data were collected with a scan width of  $0.5^\circ$ . Empirical absorption correction was performed. The structure analyses were performed by using the Crystalstructure crystallographic software package.<sup>13</sup> The structures were solved by heavy atom Patterson method by using the DIRDIF-99 program

and were expanded using Fourier techniques.<sup>14</sup> In the final cycle of the full-matrix least-squares refinement, tungsten, chromium, and silicon atoms were refined anisotropically. The other elements were refined isotropically. Neutral scattering factors were obtained from the standard source.<sup>15</sup>

**Powder X-ray Analyses.** Powder X-ray diffraction (XRD) patterns for **5a** and **2b–5b** were measured with XRD-DSCII (Rigaku Corporation) and  $Cu\ K\alpha$  radiation ( $\lambda = 1.54056\ \text{\AA}$ , 50 kV/300 mA) in a  $N_2$  flow at 303 K. The data were collected in the range of  $2\theta = 4–38^\circ$  at  $0.01^\circ$  point and 5 s/step. The lattice parameters were calculated using Materials Studio (Accelrys Inc.). The calculation was performed as follows: (i) unit cell indexing and space group determination using X-cell;<sup>16</sup> (ii) peak profile fitting using Pawley refinement;<sup>17</sup> (iii) a starting model created by arrangement of the polyoxometalates and macrocations in the unit cell, the calculated powder XRD pattern compared to the experimental data, and the model optimized by the simulated annealing method;<sup>18</sup> and (iv) final structure refinement using the Rietveld

(13) Crystal Structure 3.8.1, Structure solution, refinement, and reporting software, Rigaku/MSC, 2007.

(14) Beurskens, P. T.; Beurskens, G.; de Gelder, R.; Garcia-Granda, S.; Gold, R. O.; Israel, R.; Smits, J. M. M. *DIRDIF-99*; University of Nijmegen: Nijmegen, The Netherlands, 1999.

(15) *International Tables for X-ray Crystallography*; The Kynoch Press: Birmingham, England, 1974; Vol. 4.

(16) Neumann, M. *J. Appl. Crystallogr.* **2003**, *36*, 356.

(17) Pawley, G. S. *J. Appl. Crystallogr.* **1981**, *14*, 357.

(18) Engel, G. E.; Wilke, S.; König, O.; Harris, K. D. M.; Leusen, F. J. J. *J. Appl. Crystallogr.* **1999**, *32*, 1169.

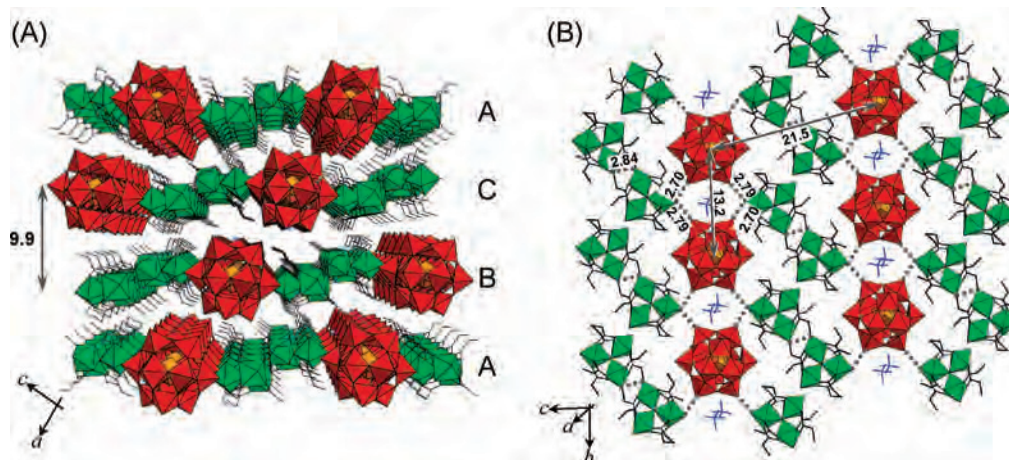


**Figure 3.** Crystal structure of  $[(\text{CH}_3)_4\text{N}]_2[\text{Cr}_3\text{O}(\text{OOCC}_2\text{H}_5)_6(\text{H}_2\text{O})_3]_2[\alpha\text{-SiW}_{12}\text{O}_{40}]\cdot 4\text{H}_2\text{O}$  [**6a**]. Perspective view (A) and arrangements of the constituent ions in the layer (B). The layers were stacked in an ABC fashion. Red, green, and orange polyhedra show the  $[\text{WO}_6]$ ,  $[\text{CrO}_6]$ , and  $[\text{SiO}_4]$ , respectively. Blue sticks show the  $(\text{CH}_3)_4\text{N}^+$ . Black sticks show the carbon chains. The water of crystallization was omitted for the clarity. Dotted lines in panel B show the hydrogen bonds in the layer.

method.<sup>19</sup> The  $R_{\text{wp}}$  values  $[\sum w(y_i - f_i)^2 / \sum w f_i^2]^{1/2}$ , where  $y_i$  and  $f_i$  are the experimental and calculated diffraction intensities, respectively, are shown in parentheses; **5a**<sup>10</sup> (18.91%), **2b** (16.41%), **3b** (18.14%), **4b** (18.64%), and **5b**<sup>10</sup> (17.14%).

**Sorption Measurements.** Ionic crystals were evacuated at 303 K for 6 h to form the corresponding guest-free phases. The liquid used to generate vapor was fully degassed by freeze–pump–thaw cycles. The sorption isotherms were measured using an automatic sorption apparatus Hydrosorb (Quantochrome Corporation), Autosorb (Quantochrome Corporation), or Omnisorb 100CX (Coulter Corporation). The saturation pressures at 298 K are shown in parentheses; water (3.16 kPa), *n*-propanol (2.73 kPa), dichloromethane (44.28 kPa), and 1,2-dichloroethane (8.84 kPa). No significant changes were observed between the first and second runs of the sorption isotherms, showing the reversibility of the vapor sorption.

**Vapor Sorption Kinetics.** Ionic crystals were treated in a dry He flow (200 mL min<sup>-1</sup>) at 303 K for 6 h to form the corresponding guest-free phases. The amounts of sorption of water ( $P/P_0 = 0.6$ ) and *n*-propanol ( $P/P_0 = 0.6$ ) were measured with a thermogravimetric analyzer Thermo Plus 2 (Rigaku Corporation) using  $\alpha\text{-Al}_2\text{O}_3$  as a reference at 298 K. No significant changes were observed between the rates and equilibrium amounts of the first and second runs.

## Results and Discussion

**Crystal Structures of 1a–6a.** The ionic crystals of **1a–6a** were prepared using  $[\alpha\text{-SiW}_{12}\text{O}_{40}]^{4-}$ ,  $[\text{Cr}_3\text{O}(\text{OOCC}_2\text{H}_5)_6(\text{H}_2\text{O})_3]^+$ , and  $\text{A}^+$  ( $\text{A} = \text{Na}$  [**1a**],  $\text{K}$  [**2a**],  $\text{Rb}$  [**3a**],  $\text{NH}_4$  [**4a**],  $\text{Cs}$  [**5a**],  $\text{TMA}$  [**6a**]) as building blocks. The elemental analyses showed the  $\text{A}^+$ /macrocation/polyoxometalate ratios of 2:2:1. The stoichiometry in the ionic crystals formed was not changed by the  $\text{A}^+$ /macrocation/polyoxometalate ratios in the synthetic solution.

Figure 1 shows the crystal structure of **1a**.<sup>20</sup> Compound **1a** consisted of 2D layers of polyoxometalates and macrocations. In the layers parallel to the *ab*-plane, macrocations and polyoxometalates were arranged in honeycomb patterns, and the distances between the oxygen atoms of adjacent macrocations and those between the oxygen atoms of polyoxometalates and macrocations were in hydrogen-bonding distances (Figure 1B). Thus, multiple hydrogen bonds as well as Coulomb interactions were observed among the constituent ions, probably stabilizing the layers. The layers were stacked along the *c*-axis with an offset of  $a/4$  with respect to each other, and the distance between the layers was 9.8 Å. Sodium ions existed between the layers.

Compounds **2a**,<sup>9</sup> **3a**, **4a**, and **5a**<sup>10</sup> had almost the same structure.<sup>21,22</sup> Figure 2 shows the crystal structure of **3a** as an example. Compound **3a** consisted of 2D layers of polyoxometalates and macrocations. In the layers parallel to the *ac*-plane, macrocations and polyoxometalates were arranged in honeycomb patterns, and the distances between the oxygen atoms of adjacent macrocations and those between the oxygen atoms of polyoxometalates and macrocations were in hydrogen-bonding distances (Figure 2B). The layers were stacked along the *b*-axis with an offset of  $a/2$  with respect to each other, and the macrocations in the adjacent layers were facing each other. Therefore, channels surrounded by the propionate ligands of macrocations were formed between the layers. The distance between the layers was 9.7 Å, and rubidium ions existed between the layers.

Figure 3 shows the crystal structure of **6a** obtained by the single-crystal X-ray analysis.<sup>23</sup> Compound **6a** consisted of 2D layers of polyoxometalates, macrocations, and TMA ions.

(21) Crystallographic data for **3a**:  $\text{C}_{36}\text{Cr}_6\text{O}_{74}\text{Rb}_2\text{SiW}_{12}$ , monoclinic  $C2/c$ ,  $a = 16.053(4)$ ,  $b = 19.460(4)$ ,  $c = 30.205(7)$ ,  $\beta = 90.944(3)$ ,  $V = 9434(4)$ ,  $Z = 4$ ,  $R1 = 0.0986$  and  $wR2 = 0.1227$  for 5383 reflections ( $I > 3\sigma(I)$ ). Two out of four molecules of the water of crystallization were located.

(22) Crystallographic data for **4a**:  $\text{C}_{36}\text{N}_2\text{Cr}_6\text{O}_{74}\text{SiW}_{12}$ , monoclinic  $C2/c$ ,  $a = 16.1365(14)$ ,  $b = 19.332(3)$ ,  $c = 30.020(4)$ ,  $\beta = 90.270(5)$ ,  $V = 9364(2)$ ,  $Z = 4$ ,  $R1 = 0.0871$  and  $wR2 = 0.0844$  for 10352 reflections ( $I > 2\sigma(I)$ ). Two out of four molecules of the water of crystallization were located.

(19) Rietveld, H. M. *J. Appl. Crystallogr.* **1969**, *2*, 65.

(20) Crystallographic data for **1a**:  $\text{C}_{36}\text{Cr}_6\text{Na}_2\text{O}_{74}\text{SiW}_{12}$ , monoclinic  $C2/c$ ,  $a = 29.8782(6)$ ,  $b = 17.6689(3)$ ,  $c = 39.0647(8)$ ,  $\beta = 93.1250(7)$ ,  $V = 20592.2(7)$ ,  $Z = 8$ ,  $R1 = 0.0740$  and  $wR2 = 0.0959$  for 14601 reflections ( $I > 2\sigma(I)$ ). Sodium ions had the occupancy of 0.5 and were disordered over the two positions. Two out of six molecules of the water of crystallization were located.

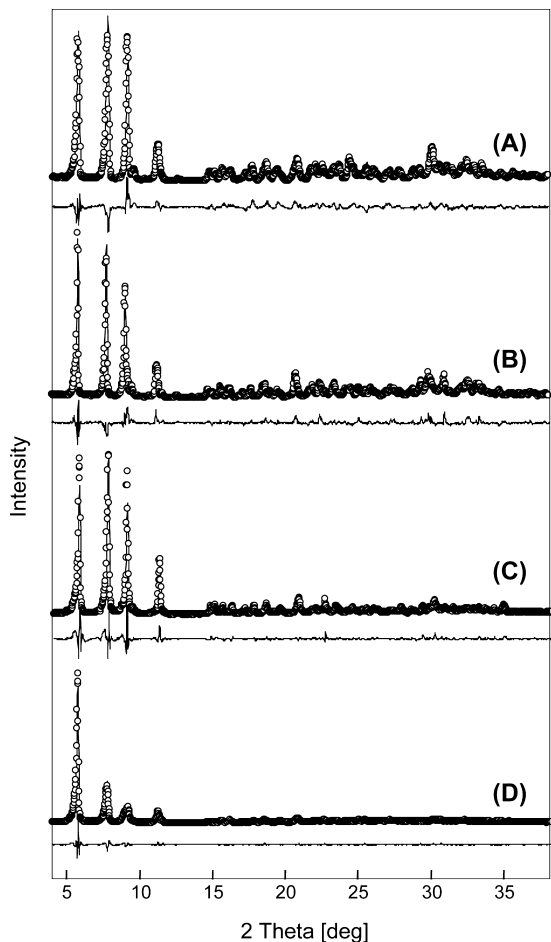


**Figure 4.** Powder X-ray diffraction patterns of (A) **2b**, (B) **3b**, (C) **4b**, and (D) **5b**. Open circles and solid lines show the observed and calculated patterns, respectively. The differences between the observed and calculated data are shown under the patterns.

In the layer, each polyoxometalate was surrounded by four macrocations. The distances between the oxygen atoms of polyoxometalates and those of macrocations were 2.70–2.79 Å and in hydrogen-bonding distances (Figure 3B). TMA ions were surrounded by two polyoxometalates and two macrocations. The layers were stacked in an ABC fashion, and the distance between the layers was 9.9 Å (Figure 3A).

**Crystal Structures of 2b–5b.**<sup>24</sup> The water of crystallization in **2a–5a** was completely desorbed by the evacuation at room temperature to form the respective guest-free phases of **2b–5b**. The powder XRD patterns of **2b–5b** are shown in Figure 4. The lattice parameters were calculated with the powder XRD patterns (Table 1). The structures of **2a–5a** were not significantly changed

**Table 1.** Structural Properties of **2b–5b**<sup>a</sup>

	<b>2b</b>	<b>3b</b>	<b>4b</b>	<b>5b</b>
<i>a</i> [Å]	15.85	15.80	15.79	15.87
<i>b</i> [Å]	19.25	19.52	19.55	19.99
<i>c</i> [Å]	30.41	30.50	30.60	30.47
<i>V</i> [Å <sup>3</sup> ]	9278	9406	9446	9667
hydrophilic channel volume [ $\mu\text{L g}^{-1}$ ]	$19.0 \pm 3.0$	$19.5 \pm 3.0$	$20.0 \pm 3.0$	$21.0 \pm 3.0$
hydrophobic channel volume [ $\mu\text{L g}^{-1}$ ]	$23.0 \pm 3.0$	$25.0 \pm 3.0$	$25.0 \pm 3.0$	$30.0 \pm 3.0$
opening [Å]	$2.5 \times 5.1$	$3.4 \times 5.1$	$3.4 \times 5.1$	$4.0 \times 5.2$

<sup>a</sup> Lattice parameters were calculated with the Rietveld analyses of the powder XRD patterns of **2b–5b** in Figure 4.

by the desorption of the water of crystallization to form **2b–5b**. Among **2b–5b**, the lengths of the *a*- and *c*-axes were not different from one another. On the other hand, the lengths of the *b*-axes, which are twice the values of the interlayer distances, increased in the order of **2b** (19.25 Å) < **3b** (19.55 Å)  $\approx$  **4b** (19.52 Å) < **5b** (19.99 Å). The increase in the lengths of the *b*-axes (i.e., interlayer distances) is probably attributed to the increase in the radii of the monovalent cations in the order of **2b** (K<sup>+</sup>: 1.52 Å) < **3b** (Rb<sup>+</sup>: 1.66 Å)  $\approx$  **4b** (NH<sub>4</sub><sup>+</sup>: 1.66 Å) < **5b** (Cs<sup>+</sup>: 1.81 Å).

**Local Structures of 2b–5b.** The local structures of **2b–5b** were investigated in more detail.<sup>10,25–27</sup> These ionic crystals possessed hydrophobic channels between the layers (Figure 5A for **3b**). The hydrophobic channels ran along the *a*-axes and were surrounded by the propionate ligands of the macrocations. The volumes of the hydrophobic channels increased in the same order of **2b** ( $23.0 \pm 3.0 \mu\text{L g}^{-1}$ ) < **3b** ( $25.0 \pm 3.0 \mu\text{L g}^{-1}$ )  $\approx$  **4b** ( $25.0 \pm 3.0 \mu\text{L g}^{-1}$ ) < **5b** ( $30.0 \pm 3.0 \mu\text{L g}^{-1}$ ) with the increase in the lengths of the *b*-axes. The opening sizes of the hydrophobic channels for **2b–5b** were  $2.5 \times 5.1$ ,  $3.4 \times 5.1$ ,  $3.4 \times 5.1$ , and  $4.0 \times 5.2$  Å, respectively.

These ionic crystals also possessed hydrophilic channels running through the layers (Figure 5B for **3b**). The hydrophilic channels contained monovalent cations and were surrounded by the polyoxometalates. The volumes of the hydrophilic channels slightly increased in the order of **2b** ( $19.0 \pm 3.0 \mu\text{L g}^{-1}$ )  $\leq$  **3b** ( $19.5 \pm 3.0 \mu\text{L g}^{-1}$ )  $\leq$  **4b** ( $20.0 \pm 3.0 \mu\text{L g}^{-1}$ ) < **5b** ( $21.0 \pm 3.0 \mu\text{L g}^{-1}$ ). The hydrophilic channels were composed of chambers with necks, and monovalent cations resided in the necks. The distances between the monovalent cations and the oxygen atoms of constituent ions in the vicinity for **2b**, **3b**, and **5b** were 2.78–3.38, 3.01–3.85, and 3.06–4.25 Å, respectively.<sup>27</sup> The sizes of the necks of **2b**, **3b**, and **5b** were estimated

(23) Crystallographic data for **6a**: C<sub>44</sub>O<sub>80</sub>N<sub>2</sub>W<sub>12</sub>SiCr<sub>6</sub>, triclinic  $P\bar{1}$ , *a* = 12.3886(4), *b* = 13.2298(5), *c* = 17.1961(13),  $\alpha$  = 88.401(9),  $\beta$  = 88.258(9),  $\gamma$  = 68.964(7), *V* = 2628.9(2), *Z* = 1, *R*1 = 0.100 and *wR*2 = 0.100 for 11429 reflections (*I* > 3 $\sigma$ (*I*)).

(24) The powder XRD pattern of **1b** largely changed from that of **1a**, and the structural analysis of **1b** was unsuccessful. The crystal structure of **6b** was solved by the powder X-ray analysis with triclinic  $P\bar{1}$ , *a* = 17.20, *b* = 12.68, *c* = 12.12,  $\alpha$  = 115.07,  $\beta$  = 97.95,  $\gamma$  = 88.34, and *V* = 2370 (*R*<sub>w</sub> = 20.65%). In **6b**, polyoxometalates and macrocations individually formed layers which stacked alternately along the *a*-axis, and the structure was different from those of **2b–5b** (monoclinic,  $C2/c$ ). Therefore, the structures and sorption properties of **1b** and **6b** could not be discussed along with **2b–5b**.

(25) Crystallographic data for **2b**: C<sub>36</sub>Cr<sub>6</sub>K<sub>2</sub>O<sub>72</sub>SiW<sub>12</sub>, monoclinic  $C2/c$ , *a* = 15.7371(5), *b* = 19.1665(5), *c* = 30.8544(11),  $\beta$  = 90.7324(10), *V* = 9305.7(5), *Z* = 4, *R*1 = 0.081 and *wR*2 = 0.1040 for 11418 reflections (*I* > 2 $\sigma$ (*I*)).

(26) Crystallographic data for **3b**: C<sub>36</sub>Cr<sub>6</sub>O<sub>72</sub>Rb<sub>2</sub>SiW<sub>12</sub>, monoclinic  $C2/c$ , *a* = 15.9888(17), *b* = 19.3842(18), *c* = 30.193(3),  $\beta$  = 90.856(5), *V* = 9356.7(17), *Z* = 4, *R*1 = 0.1331 and *wR*2 = 0.1324 for 13113 reflections (*I* > 2 $\sigma$ (*I*)).

(27) Powder X-ray analysis showed that the structure of **4b** was almost the same as those of **2b**, **3b**, and **5b**. The volumes and openings of the hydrophilic and hydrophobic channels of **4b** could be estimated as shown in Table 1, while the ammonium ions could not be located because of the small X-ray scattering as compared with polyoxometalates, macrocations, and alkali metal ions.

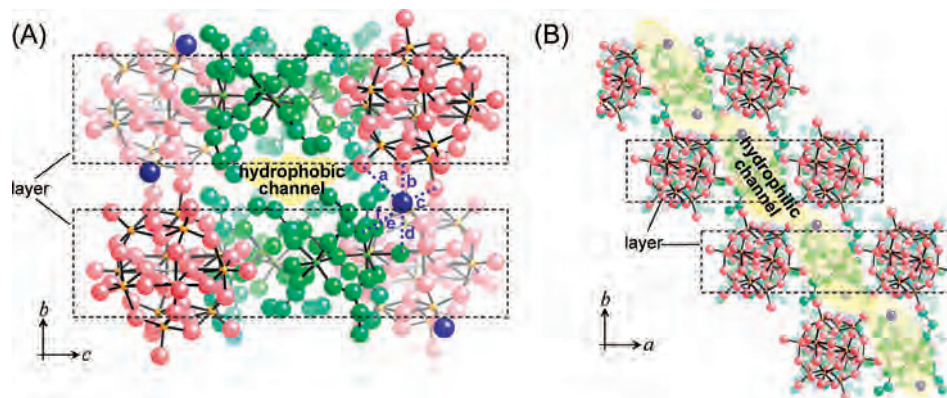


**Figure 5.** Local structures of  $\text{Rb}_2[\text{Cr}_3\text{O}(\text{OOCC}_2\text{H}_5)_6(\text{H}_2\text{O})_3]_2[\alpha\text{-SiW}_{12}\text{O}_{40}]$  [**3b**] in the (A)  $bc$ - and (B)  $ab$ -plane. Pink, yellow-green, green, and blue spheres show the oxygen atoms of polyoxometalate, oxygen atoms of the macrocation, carbon atoms, and alkali metal ions, respectively. Small orange and small green spheres show the tungsten and chromium atoms, respectively. Dashed rectangles show the layers. Hydrophilic and hydrophobic channels are indicated by the yellow shadings. Distances in panel A between the rubidium ions and the oxygen atoms in the vicinity were a: 3.34 Å, b: 3.01 Å, c: 3.85 Å, d: 3.04 Å, e: 3.07 Å, and f: 3.10 Å.

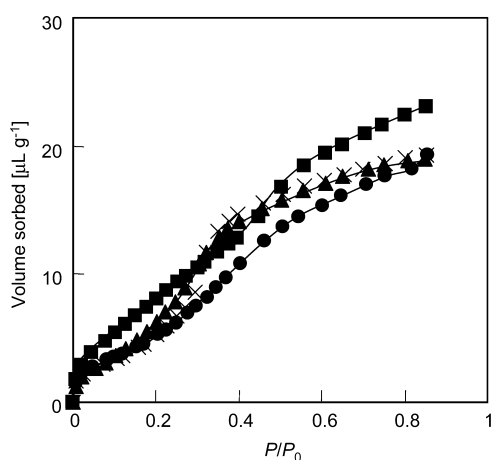


**Figure 6.** Water vapor sorption isotherms of **2b** (solid circle), **3b** (solid triangle), **4b** (cross), and **5b** (solid square) at 298 K.

to be  $3.2 \times 4.4$ ,  $3.2 \times 4.6$ , and  $3.3 \times 4.8$  Å, respectively. Therefore, the cross section areas of the necks increased in the order of **2b** < **3b** < **5b**, and it is probable that guest molecules are more easily sorbed into the hydrophilic channels of **5b** than **2b**.

**Water Vapor Sorption Properties.** Figure 6 shows the water vapor sorption isotherms for **2b–5b** (298 K). The amounts of sorption increased with the increase in the water vapor pressure and were almost leveled off around  $P/P_0 = 0.8$ . The amounts around  $P/P_0 = 0.8$  reached up to 19–22  $\mu\text{L g}^{-1}$  and approximately agreed with the volumes of the hydrophilic channels (19–21  $\mu\text{L g}^{-1}$ ).

The changes in the amounts of water sorption for **2b–5b** at 298 K and  $P/P_0 = 0.60$  as a function of time are shown in Figure 7. As for **2b**, **3b**, and **5b**, the amounts gradually increased and were almost leveled off after 300 s. The profiles could be reproduced by the linear driving force mass transfer model,<sup>28</sup>

$$M_t = M_e \{1 - \exp(-k_1 t)\} \quad (1)$$

where  $M_t$  and  $M_e$  are the amounts of sorption at time  $t$  and equilibrium, respectively, and  $k_1$  is the rate constant. The parameters of the best fits for the water sorption by **2b–5b**

are summarized in Table 2, and the water sorption profiles of **2b–5b** were approximately reproduced by the eq 1. Single-crystal X-ray structure analyses of **2a**,<sup>9</sup> **3a**,<sup>21</sup> and **4a**<sup>22</sup> have shown that the water of crystallization resides in the hydrophilic channel. It is probable for **5a** that the water molecules reside in the hydrophilic channel in the same manner as those of **2a–4a** since **2a–5a** had almost the same structure. Therefore, water molecules sorbed in **2b–5b** probably reside in the hydrophilic channel. The  $M_e$  values increased in the same order of **2b** < **3b** < **4b** ≤ **5b** as that of the volumes of the hydrophilic channels. The  $k_1$  values changed in the order of **4b** < **2b** < **3b** < **5b**. The smallest rate constant and small deviation observed between the experimental and calculated profiles for **4b** may be due to the hydrogen-bonding ability of the ammonium ion in **4b**. The  $k_1$  values among **2b**, **3b**, and **5b** changed in the same order as that of the cross section areas of the necks of the hydrophilic channels.

***n*-Propanol Vapor Sorption Properties.** Figure 8 shows the *n*-propanol vapor sorption isotherms for **2b–5b** at 298 K. The amounts at  $P/P_0 > 0.6$  exceeded the volumes of the hydrophilic channel and reached up to 30, 35, 45, and 55  $\mu\text{L g}^{-1}$  for **2b**, **3b**, **4b**, and **5b**, respectively, and were larger than each volume of hydrophilic or hydrophobic channel.<sup>29</sup> This fact suggests that amphiphilic alcohols are sorbed into both hydrophilic (19–21  $\mu\text{L g}^{-1}$ ) and hydrophobic (23–30  $\mu\text{L g}^{-1}$ ) channels.<sup>30</sup>

(29) The amounts of *n*-propanol sorbed exceeded the sum of the volumes of the hydrophilic and hydrophobic channels for **3b** (45  $\mu\text{L g}^{-1}$ ) at  $P/P_0 > 0.8$  and 0.6, respectively. Upon the exposure of **3b** and **5b** to the saturated *n*-propanol vapor, the powder XRD patterns initially showed peaks attributable to the phases with expansion in the lengths of the  $b$ -axes. Then, drastic changes in the whole profiles were observed, indicating the transformation into unidentified phases.

(30) Compounds **2b–5b** sorbed *n*-propanol (cross section diameter ( $d$ ) = 4.6 Å), while larger *t*-butanol ( $d$  = 5.0 Å) was excluded.<sup>31</sup>

(31) The cross section diameter of the molecule was defined as the diameter of the circumscribed circle of the smallest cross section of the molecular model. The molecular model was calculated with the van der Waals radii of the elements. These calculated values agreed with those reported in ref 32.

(32) McClellan, A. L.; Harnsberger, H. F. *J. Colloid Interface Sci.* **1967**, *23*, 577.

(33) Fletcher, A. J.; Cussen, E. J.; Bradshaw, D.; Rosseinsky, M. J.; Thomas, K. M. *J. Am. Chem. Soc.* **2004**, *126*, 9750.

(28) Foley, N. J.; Thomas, K. M.; Forshaw, P. L.; Stanton, D.; Norman, P. R. *Langmuir* **1997**, *13*, 2083.

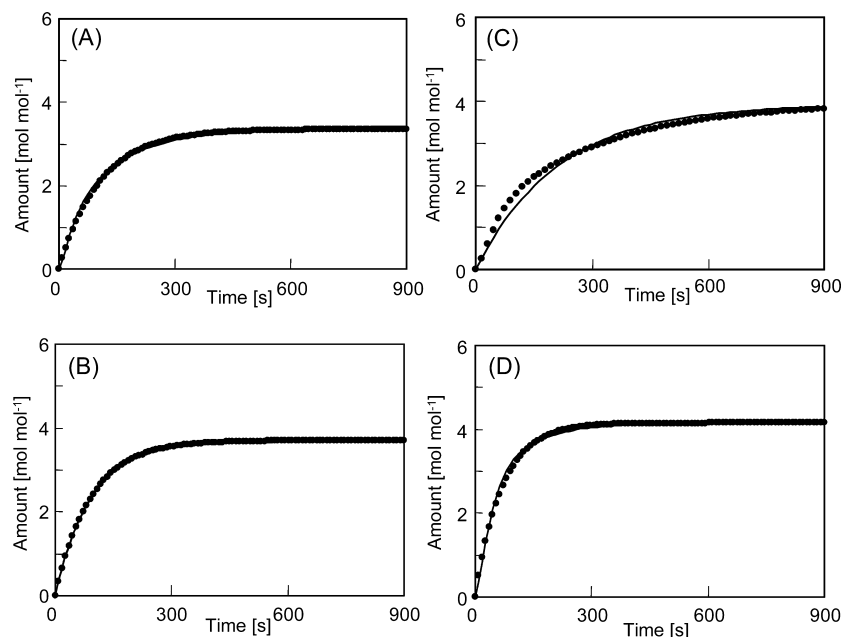


**Figure 7.** Changes in the amounts of water vapor sorption for (A) **2b**, (B) **3b**, (C) **4b**, and (D) **5b** at 298 K as a function of time ( $P/P_0 = 0.60$ ). The solid line shows the experimental data, and solid circles show the calculated data according to the eq 1.

**Table 2.** Kinetic Parameters ( $M_{e1}$  [ $\mu\text{L g}^{-1}$ ] (mol mol $^{-1}$ ) and  $k_n$  [ $\text{s}^{-1}$ ]) of Water and *n*-Propanol Sorption at 298 K and  $P/P_0 = 0.60$

	$M_{e1}$	$k_1$	$M_{e2}$	$k_2$	$M_{e1}:M_{e2}^a$
Water					
<b>2b</b>	13.7 (3.35)	$9.20 \times 10^{-3}$			
<b>3b</b>	14.9 (3.70)	$1.08 \times 10^{-2}$			
<b>4b</b>	16.5 (3.93)	$4.68 \times 10^{-3}$			
<b>5b</b>	16.6 (4.15)	$1.42 \times 10^{-2}$			
<i>n</i> -Propanol					
<b>2b</b>	14.8 (0.85)	$8.54 \times 10^{-4}$	7.1 (0.40)	$2.90 \times 10^{-4}$	0.68:0.32 (0.72:0.28)
<b>3b</b>	18.7 (1.07)	$8.22 \times 10^{-4}$	13.2 (0.75)	$2.92 \times 10^{-4}$	0.59:0.41 (0.62:0.38)
<b>4b</b>	19.2 (1.10)	$4.16 \times 10^{-4}$	16.6 (0.95)	$6.56 \times 10^{-5}$	0.54:0.46
<b>5b</b>	22.5 (1.29)	$7.25 \times 10^{-4}$	24.3 (1.39)	$1.35 \times 10^{-4}$	0.48:0.52 (0.49:0.51)

<sup>a</sup> Figures in parentheses are integrated intensity ratios of 3250–3270  $\text{cm}^{-1}$  bands to 3340–3360  $\text{cm}^{-1}$  bands.

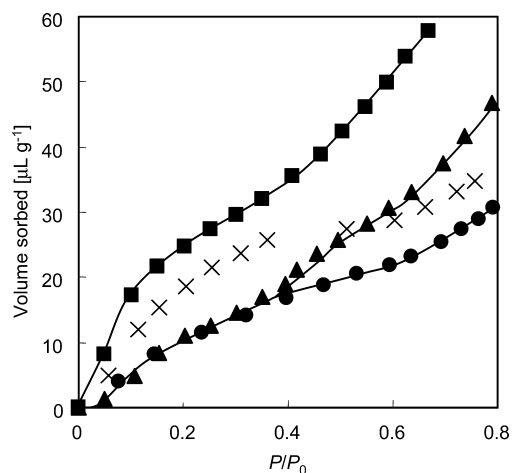


**Figure 8.** *n*-Propanol vapor sorption isotherms of **2b** (solid circle), **3b** (solid triangle), **4b** (cross), and **5a** (solid square) at 298 K.

The changes in the amounts of *n*-propanol sorption for **2b**–**5b** at 298 K and  $P/P_0 = 0.60$  as a function of time are shown in Figure 9. In contrast with the water sorption, the amounts for the *n*-propanol sorption gradually increased. The sorption could not be reproduced by eq 1. Therefore, two kinds of barriers were considered according to eq 2, as in

the case of the alcohol sorption for the Ni-bipyridine compound.<sup>33</sup>

$$M_t = M_{e1}\{1 - \exp(-k_1t)\} + M_{e2}\{1 - \exp(-k_2t)\} \quad (2)$$

where  $M_{e1}$  and  $M_{e2}$  are the contributions of the each of the two processes controlling the overall sorption (i.e.,  $M_{e1} + M_{e2} = M_e$ : amounts of sorption at equilibrium), and  $k_1$  and  $k_2$  are the rate constants. The parameters of the best fits for the *n*-propanol sorption by **2b**–**5b** are summarized in Table 2. The  $M_{e1}$  and  $M_{e2}$  values increased in the order of **2b** < **3b** < **4b** < **5b**, and the order was the same as those of the volumes of the hydrophilic and hydrophobic channels.

The in situ IR spectra of **2b**, **3b**, and **5b** under *n*-propanol vapor ( $P/P_0 = 0.6$  at 298 K) were measured, and the difference spectra between the compounds before and after the sorption were deconvoluted to investigate the states of *n*-propanol sorbed (Figure S1). The IR spectra of the  $\nu(\text{OH})$  region consisted of two bands at 3340–3360 and 3250–3270  $\text{cm}^{-1}$ . In general, the  $\nu(\text{OH})$  band of alcohol molecules shifts to the lower wavenumbers with the formation of hydrogen bonds.<sup>34</sup> Of the two types of channels, hydrophilic channels

(34) Pimentel, G. C.; McClellan, A. L. *The Hydrogen Bond*; W. H. Freeman and Co.: San Francisco and London, 1960; Chapter 3.

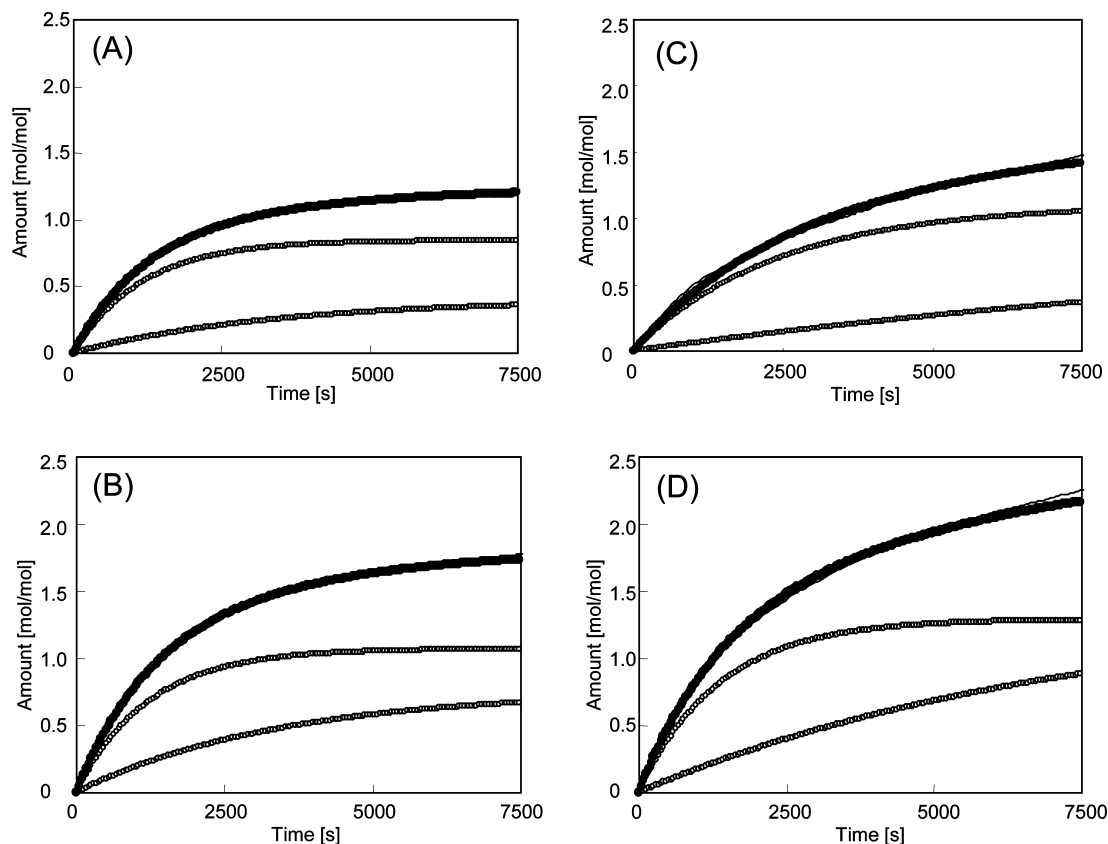


**Figure 9.** Changes in the amounts of *n*-propanol vapor sorption for (A) **2b**, (B) **3b**, (C) **4b**, and (D) **5b** at 298 K as a function of time ( $P/P_0 = 0.60$ ). The solid lines show the experimental data. The solid circles show the calculated data according to eq 2. Open circles show the two components for the calculation.

surrounded by the polyoxometalates probably possess stronger hydrogen-bonding ability.<sup>9</sup> Therefore, it is probable that the 3250–3270 and 3340–3360  $\text{cm}^{-1}$  bands are assigned to the  $\nu(\text{OH})$  bands of *n*-propanol in the hydrophilic and hydrophobic channels, respectively. The integrated band intensity ratios for **2b**, **3b**, and **5b** were 0.72:0.28, 0.62:0.38, and 0.49:0.51, respectively. These ratios approximately agreed with  $M_{e1}:M_{e2}$  ratios (Table 2), supporting the idea. Therefore, the  $M_{e2}$  and  $k_2$  values probably explain the sorption of *n*-propanol into the hydrophobic channel, while  $M_{e1}$  and  $k_1$  values probably explain those into the hydrophilic channel. Thus, the sorption kinetic and IR data show that amphiphilic *n*-propanol is sorbed into both hydrophilic and hydrophobic channels.

The *n*-propanol sorption profiles of **2b**, **3b**, and **5b** at 298 K and  $P/P_0 = 0.20$  were also reproduced by eq 2 (Figure S2). The  $M_{e1}:M_{e2}$  ratios for **2b**, **3b**, and **5b** were 0.79:0.21, 0.69:0.31, and 0.62:0.38, respectively (Table S1). The ratios of  $M_{e1}$  to  $M_{e2}$  increased with the decrease in the *n*-propanol vapor pressure, which was also confirmed by the IR spectroscopy (Figure S3). Therefore, *n*-propanol molecules are probably more preferentially sorbed into the hydrophilic channels at lower pressures, and the same phenomenon was observed for the ethanol sorption by **2b**.<sup>9</sup>

Compounds **2b**, **3b**, and **5b** sorbed *n*-butanol and butylnitrile as well as *n*-propanol, and it was shown that the amounts of sorption increased in the order of  $\mathbf{2b} \leq \mathbf{3b} < \mathbf{5b}$  (Figure S4).

**Halocarbon Vapor Sorption Properties.** Figure 10 shows the dichloromethane and dichloroethane vapor sorption isotherms of **2b–5b**. Compound **5b** sorbed dichloromethane and dichloroethane, while the amounts for **2b–4b** were comparable to or smaller than those of surface adsorption ( $< 5 \mu\text{L g}^{-1}$ ). This is probably because the opening of the hydrophobic channel of **5b** ( $4.0 \times 5.2 \text{ \AA}$ ) was large enough to accommodate dichloromethane ( $d = 4.2 \text{ \AA}$ ) and 1,2-dichloroethane ( $d = 4.5 \text{ \AA}$ ), while those of **2b** ( $2.5 \times 5.1 \text{ \AA}$ ), **3b** ( $3.4 \times 5.1 \text{ \AA}$ ), and **4b** ( $3.4 \times 5.1 \text{ \AA}$ ) were too small.<sup>31,35</sup> The amount of dichloromethane sorption for **5b** around the saturation pressure at 273 K was  $25 \mu\text{L g}^{-1}$ , which fairly agreed with the volume of the hydrophobic channel of **5b** ( $30.0 \pm 3.0 \mu\text{L g}^{-1}$ ) in accord with the idea that hydrophobic halocarbons are sorbed only in the hydrophobic channel.

## Conclusion

A series of ionic crystals and the respective guest-free phases composed of Keggin-type polyoxometalate ( $[\alpha\text{-SiW}_{12}\text{O}_{40}]^{4-}$ ), macrocation ( $[\text{Cr}_3\text{O}(\text{OCC}_2\text{H}_5)_6(\text{H}_2\text{O})_3]^+$ ), and monovalent cation ( $A^+ = \text{Na}^+, \text{K}^+, \text{Rb}^+, \text{NH}_4^+, \text{Cs}^+$ , and  $\text{TMA}^+$ ) were synthesized. The structures were solved by the single-crystal and/or powder XRD analyses, and the vapor sorption properties were investigated by the sorption iso-

(35) Compound **5b** sorbed dichloromethane ( $d = 4.2 \text{ \AA}$ ) and 1,2-dichloroethane ( $d = 4.5 \text{ \AA}$ ), while larger chloroform ( $d = 4.8 \text{ \AA}$ ) and 1,2-dichloropropane ( $d = 4.8 \text{ \AA}$ ) were excluded.<sup>31</sup>

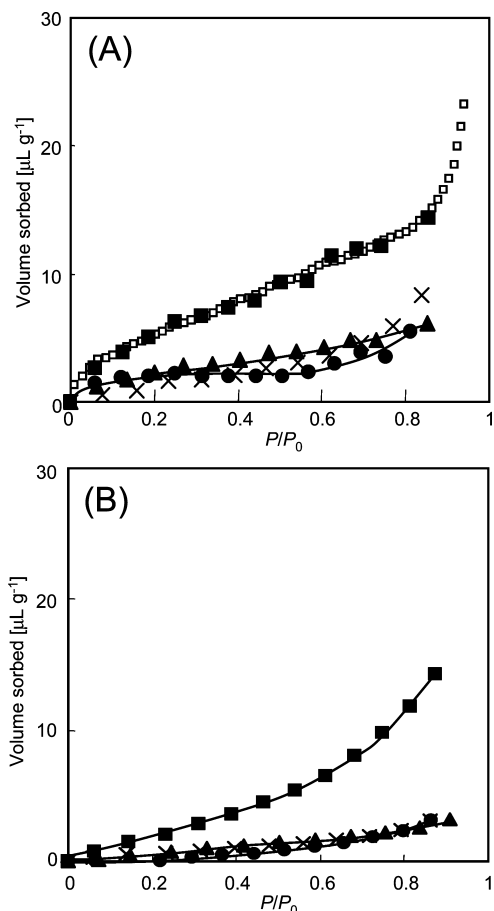


**Figure 10.** (A) Dichloromethane and (B) dichloroethane vapor sorption isotherms of **2b** (solid circle), **3b** (solid triangle), **4b** (cross), and **5b** (solid square) at 298 K. Open squares in (A) show the results at 273 K for **5b**.

therms, sorption kinetics, and in situ IR spectroscopy. It was shown that the ionic crystals possessed 2D layers of

polyoxometalates and macrocations. Ionic crystals with  $K^+$ ,  $Rb^+$ ,  $NH_4^+$ , and  $Cs^+$  had almost the same structure and possessed hydrophilic and hydrophobic channels. The volumes and opening sizes of the channels increased with the increase in the radii of the monovalent cations which resided between the layers. It was shown that water and halocarbons were sorbed in the hydrophilic and hydrophobic channels, respectively, while *n*-propanol was sorbed in both channels, and that the rates and equilibrium amounts of vapor sorption systematically changed depending on the volumes and opening sizes of the channels. All of these results showed the control of structure and sorption of hydrophilic (water), amphiphilic (*n*-propanol), and hydrophobic (halocarbons) molecules by the sizes of the monovalent cations in the ionic crystal.

**Acknowledgment.** This work was supported in part by the Core Research for Evolutional Science and Technology (CREST) program of the Japan Science and Technology Agency (JST) and Grant-in-Aid for Scientific Research from the Ministry of Education, Culture, Sports, Science, and Technology of Japan.

**Supporting Information Available:** X-ray crystallographic files of **1a–6a** and **2b–5b** in CIF format, IR spectra ( $3000\text{--}3600\text{ cm}^{-1}$ ) of *n*-propanol sorbed by **2b**, **3b**, and **5b** at 298 K and  $P/P_0 = 0.6$  (Figure S1), changes in the amounts of *n*-propanol vapor sorption for **2b**, **3b**, and **5b** at 298 K as a function of time ( $P/P_0 = 0.20$ ) (Figure S2), kinetic parameters of *n*-propanol sorption at 298 K and  $P/P_0 = 0.20$  (Table S1), IR spectra ( $3000\text{--}3600\text{ cm}^{-1}$ ) of *n*-propanol sorbed by **2b** at 298 K and  $P/P_0 = 0.2$  (Figure S3), and *n*-butanol and butyronitrile vapor sorption isotherms at 298 K (Figure S4). This material is available free of charge via the Internet at <http://pubs.acs.org>.

IC702333W